EM Implosion Memos

Memo 51

July, 2010

Experimental results for the focal waveform and beam width in the focusing lens with a 100 ps filter

Prashanth Kumar, Carl E. Baum, Serhat Altunc, Christos G. Christodoulou and Edl Schamiloglu
University of New Mexico
Department of Electrical and Computer Engineering
Albuquerque, NM 87131

Abstract

This paper presents experimental results for the focal waveform and beam width in the focusing lens with a 100 ps filter. The calibration of the D-dot probe in the target medium is explained. The electric enhancement of the focal impulse in the lens is determined. It is shown that the focusing lens acts as a band pass filter. The experimental results are found to agree well with analytical calculations and numerical simulations.

1 Introduction

Experimental results for the focusing lens with a 45 ps pulser were presented in [1]. It was assumed that the lens filtered high frequency (> 10 GHz) components in the input signal, i.e., adding a filter with a 100 ps time constant would not affect the FWHM of the focal impulse. Therefore, the focal impulse, and beam width, inside the focusing lens were not rescaled, as done for the results in air [1]. This paper presents more accurate experimental results in the focusing lens with the 100 ps filter described in [2].

2 Calibration of the D-dot probe in target medium

The calibration of the handmade D-dot probe [1] in the target medium is more complicated as an "infinitely" large sample is not available. The probe is calibrated in the target medium using only the slab for measurement as shown in Fig. 2.2. The probe is inserted between a slit cut in the slab, Fig. 2.1. The relative permittivity of the target medium is known from previous measurements, $\epsilon_{rt} = 8.2$. The theoretical value of the prepulse inside the target medium is

$$E_{pt} = TE_{pa}, \tag{2.1}$$

where T is the transmission coefficient from air into the target medium,

$$T = \frac{2}{1 + \sqrt{\epsilon_{rt}}}, \tag{2.2}$$

and ϵ_{rt} is the relative permittivity of the target medium. The prepulse measured by the probe, normalized to a 1 V input, is

$$E_{pt}^{\text{measured}} = \frac{1}{20T\epsilon_0\epsilon_{rt}Z_cA_{eq}} \int_{-\infty}^{t} V(t')dt'. \tag{2.3}$$

We require that the measured prepulse be $E_{pt} = TE_{pa}$. For this we multiply the measured electric field by the calibration factor, $\mathcal{C}_t$,

$$\mathcal{C}_t = \frac{E_{pt}}{E_{pt}^{\text{measured}}} = \left(\frac{2}{1 + \sqrt{\epsilon_{rt}}}\right) \frac{E_{pa}}{E_{pt}^{\text{measured}}}. \tag{2.4}$$

where $E_{pa} = -0.7$ V/m is the analytical value of the prepulse in air.

Figure 2.3 shows the schematic to calibrate the probe inside the target medium (slab). The width of the slab is d_t cm. Consequently, the prepulse inside the slab, $E_{pt} = TE_{pa}$, undergoes reflections at the slab boundary. The reflected wave, $E_{pt}^r = \Gamma E_{pt}$, interferes with the direct wave, E_{pt}, after the round trip time t_p; Γ is the reflection coefficient. Therefore, for times $t > t_p$, E_{pt} cannot be used to calibrate the probe as the analytical value of the prepulse is not known. In Fig. 2.3, d' is the distance between the probe tip, on the surface of the brass mount, and geometrical second focal point. The round trip time, t_p, of the reflected wave is

$$t_p = \frac{2(d_t - d')\sqrt{\epsilon_{rt}}}{c}, \tag{2.5}$$

where c is the speed of light in vacuum.

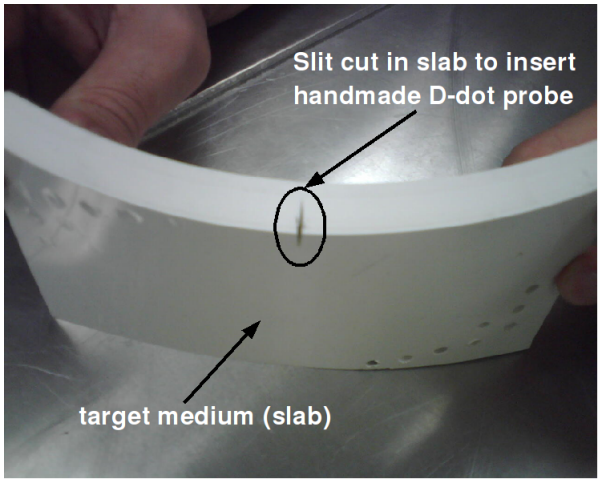

Figure 2.1: Slit cut in target medium/slab into which the handmade D-dot probe is inserted.

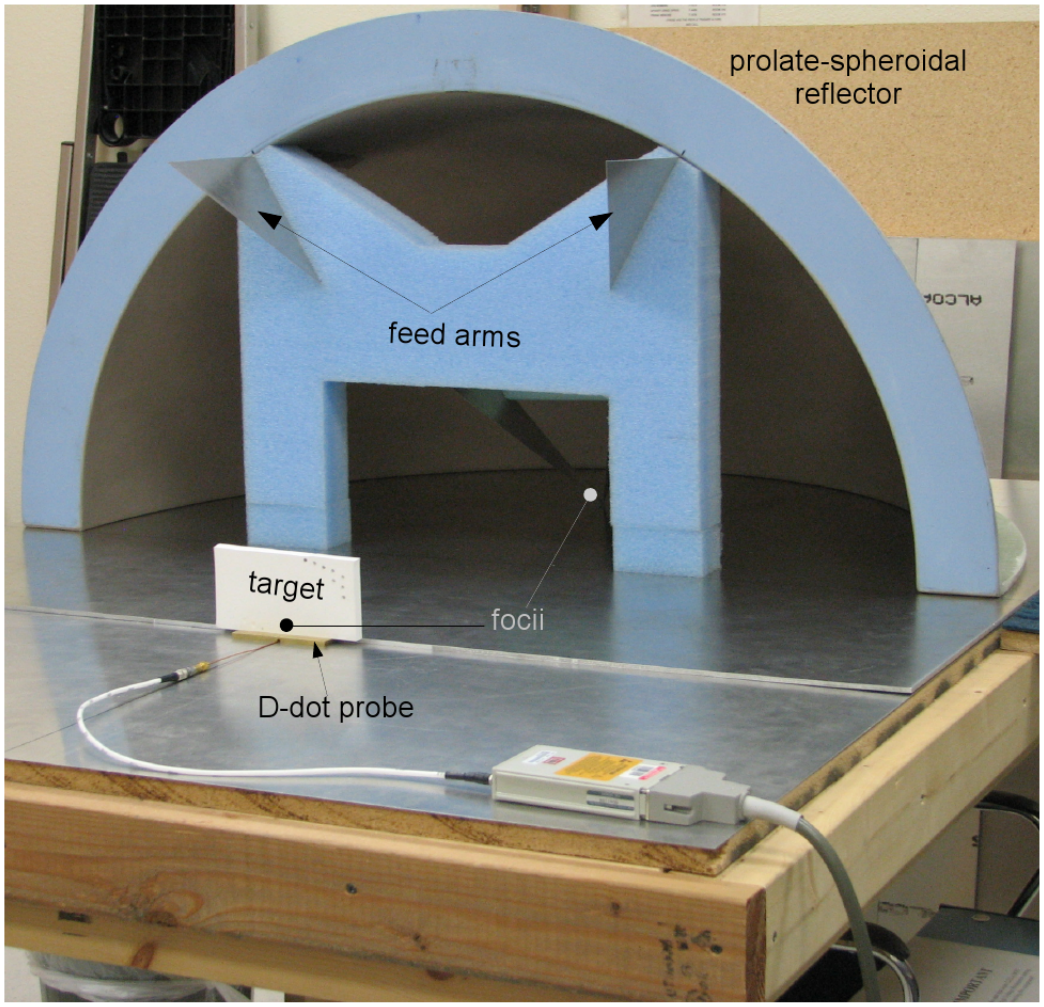

Figure 2.2: Setup to calibrate D-dot probe inside dielectric medium.

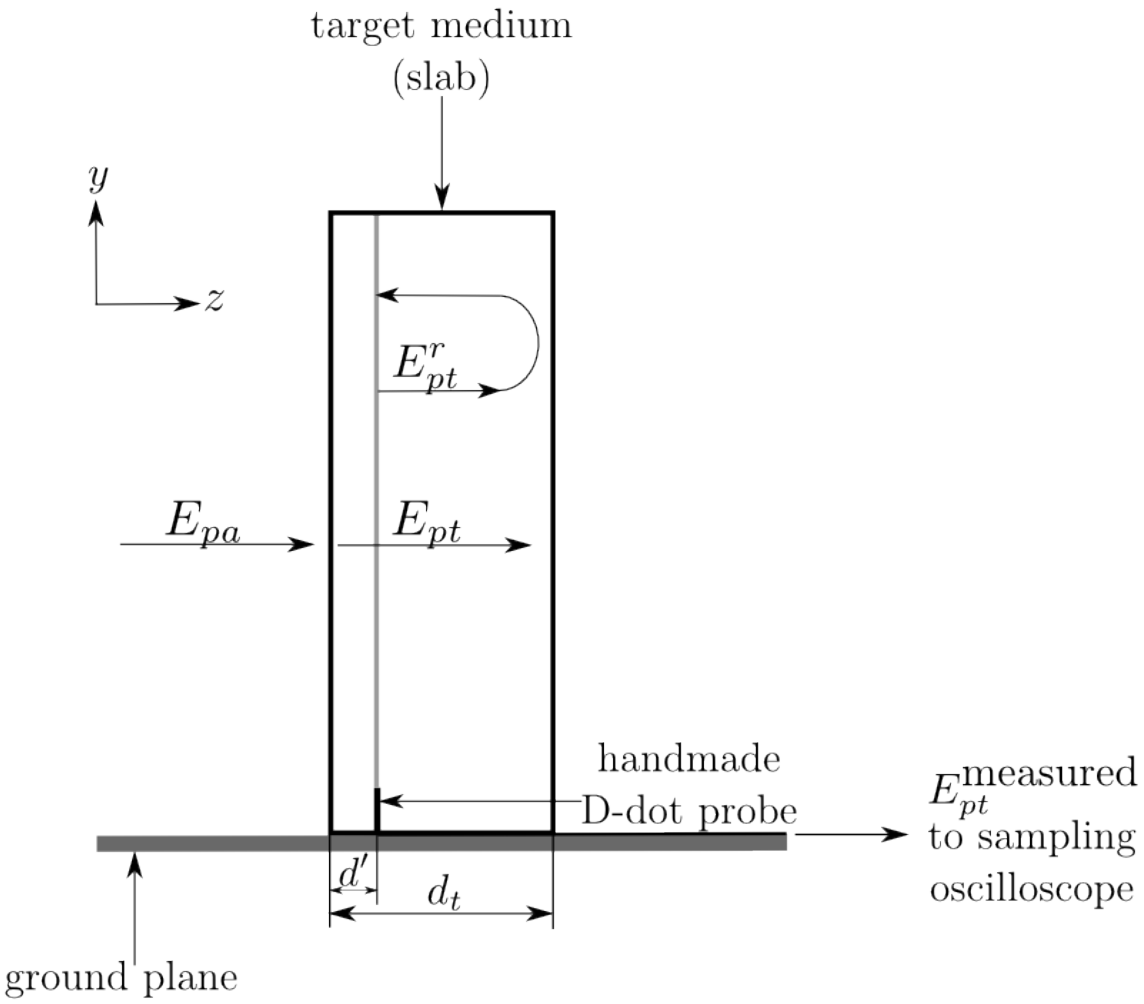

Figure 2.3: Schematic to calibrate D-dot probe.

Given that $d' \approx 0.3$ cm and $d_t \approx 1.27$ cm $\Rightarrow t_p \approx 187.42$ ps, i.e., only the first ≈ 200 ps of the prepulse inside the slab can be used to calibrate the D-dot probe. The electric field response and the "zoomed-in" prepulse are shown in Fig. 2.4.

When the probe is inside the target medium, the time taken for the wave to reach the probe is

$$\frac{75 \text{ cm}}{3 \times 10^8 \text{ cm/s}} + \frac{(0.3 \text{ cm})\sqrt{8.4}}{3 \times 10^8 \text{ cm/s}} \approx 2.53 \text{ ns} \tag{2.6}$$

As in [2], the focal waveform in Fig. 2.4 is time-shifted so that the prepulse starts at 2.53 ns.

The D-dot probe is designed to have a pulse impedance of 50 Ω in the dielectric medium, i.e., 150 Ω in air. The impedance mismatch between the probe tip and the input pulse in air causes reflections. However, the probe, of height $h = 3$ mm, is resonant at frequencies above

$$f \approx \frac{c}{h/4} = \frac{3 \times 10^{11} \text{ mm}}{0.75 \text{ mm}} = 0.4 \text{ THz}, \tag{2.7}$$

i.e., in a quasi-static sense, the measurements are valid over a very large frequency spectrum of the input pulse and can therefore be considered sufficiently accurate.

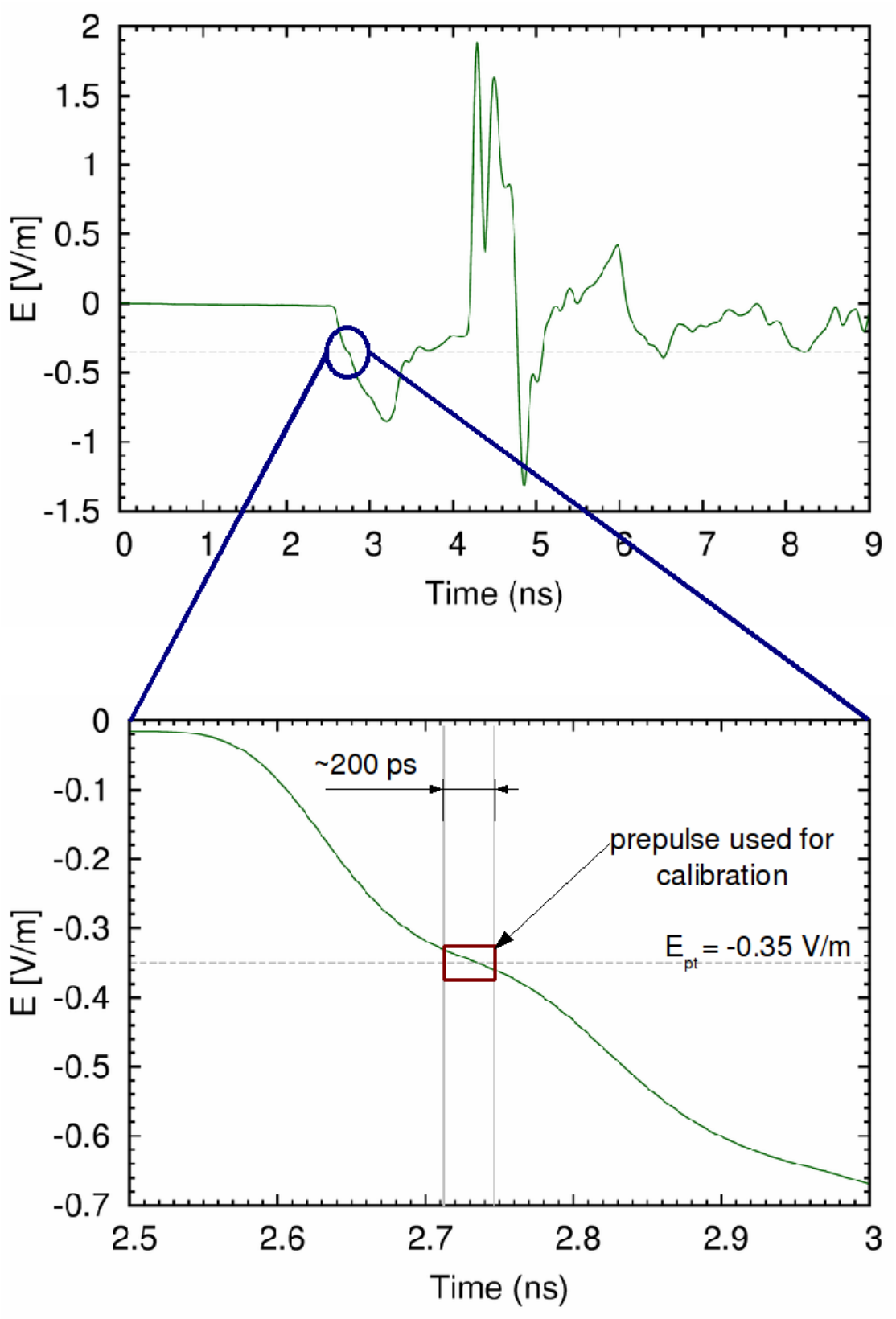

Figure 2.4: Electric field measured by D-dot probe inside slab (top); "zoomed-in" prepulse used for calibrating D-dot probe inside target medium (bottom).

3 Experimental Setup

The setup to measure the focal impulse waveform and the beam width in the focusing lens is identical to that in [2] except that the focusing lens and target medium are placed between the PSIRA and the D-dot probe as shown in the block diagram in Fig. 3.1. The details of the components used in the experiments are given in [1].

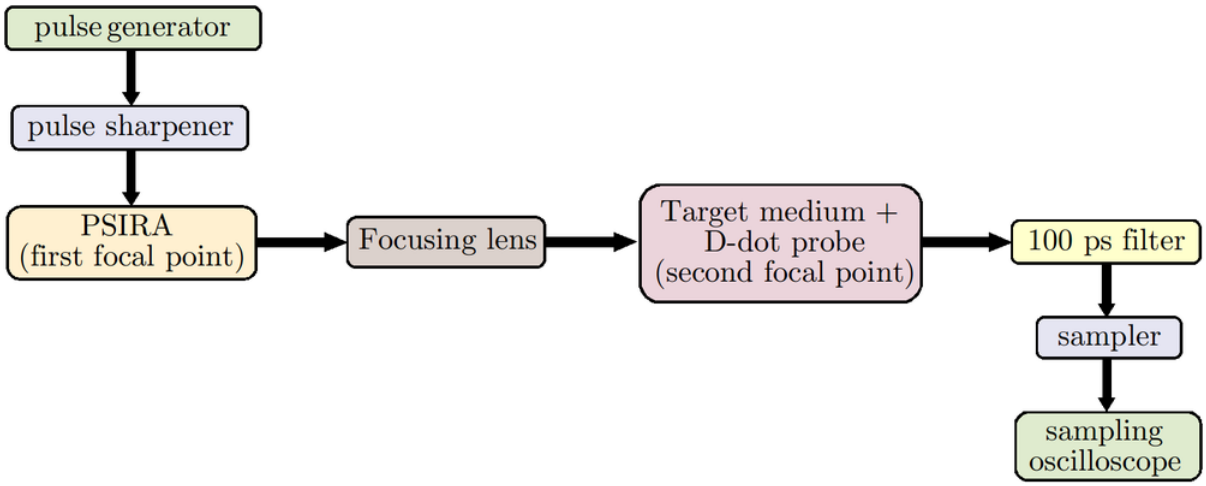

Figure 3.1: Block diagram of the experimental setup with the focusing lens and 100 ps filter.

4 Results

4.1 Focal impulse waveform

The raw and integrated D-dot probe signals, at the second focal point, in the focusing lens, with the 100 ps filter are shown in Fig. 4.1. The corresponding electric field focal impulse waveform is shown in Fig. 4.2.

The radii and relative dielectric constants of the layers for the focusing lens are summarized in Table. 1.

Table 1: Dimensions and relative dielectric constants for the five layers of the focusing lens.

Layer #	Radius (cm) $[r_n]$	ϵ_{r_n}
1	15.0	1.60
2	12.0	2.40
3	9.70	3.74
4	7.80	5.80
5	6.20	9.00

The distance from the first focal point to the outermost layer of the focusing lens is $D = 75.0 - 15.0 = 60.0$ cm. Therefore, the theoretical time taken for the wave to travel from the source, through the focusing lens, to the probe tip, located $d' = 0.3$ cm in the target medium/slab, is

$$\frac{D + \sum_{n=1}^{5} d_n \sqrt{\epsilon_{r_n}} + d' \sqrt{\epsilon_{r_5}}}{c}. \tag{4.1}$$

where d_n is the radius of the n^{th} "shell", i.e., $d_n = r_n - r_{n-1}$, and ϵ_{r_n} is the relative dielectric constant of the n^{th} layer. The time taken for the wave to travel,

- From the first focal point to the outermost layer of focusing lens is

$$t_1 = \frac{D}{c} = \frac{60.0 \text{ cm}}{3 \times 10^{10} \text{ cm/s}} = 2.0 \text{ ns}. \tag{4.2}$$

- From outermost layer of focusing lens to the second focal point is

$$t_2 = \frac{\sum_{n=1}^{5} d_n \sqrt{\epsilon_{r_n}}}{c} \tag{4.3}$$

$$= \left[\frac{((15.0 - 12.0)\sqrt{1.6} + (12.0 - 9.70)\sqrt{2.40} + (9.70 - 7.80)\sqrt{3.74}) \text{ cm}}{3 \times 10^{10} \text{ cm/s}} \right] + \left[\frac{((7.80 - 6.20)\sqrt{5.80} + 6.2\sqrt{9.0}) \text{ cm}}{3 \times 10^{10} \text{ cm/s}} \right] = 1.116 \text{ ns}. \tag{4.4}$$

- From the second focal point to the probe tip in the target medium/slab is

$$t_3 = \frac{d' \sqrt{\epsilon_{r_5}}}{c} = \frac{0.3 \sqrt{9.0} \text{ cm}}{3 \times 10^{10} \text{ cm/s}} = 30 \text{ ps}. \tag{4.5}$$

The total time for a wave launched from the first focal point to reach the probe tip is $\tau_p = t_1 + t_2 + t_3 \approx 3.146$ ns. Note that τ_p is analytical, i.e., $\epsilon_{rt} = \epsilon_{r5} \neq 8.2$. As in [2], since there is no time of reference in the experiments, the plots in Fig. 4.1(b) and Fig. 4.2 are shifted so that the prepulse starts at 3.146 ns.

Similar to the results in [1], one observes that in Fig. 4.2 the prepulse is dispersed, as the lens is not designed to focus this part of the waveform. This is advantageous as it increases the amplitude of the impulse. One also notes the large negative area in the post pulse (low frequencies). The lower frequencies in the input pulse are filter due to the to the geometry of the lens.

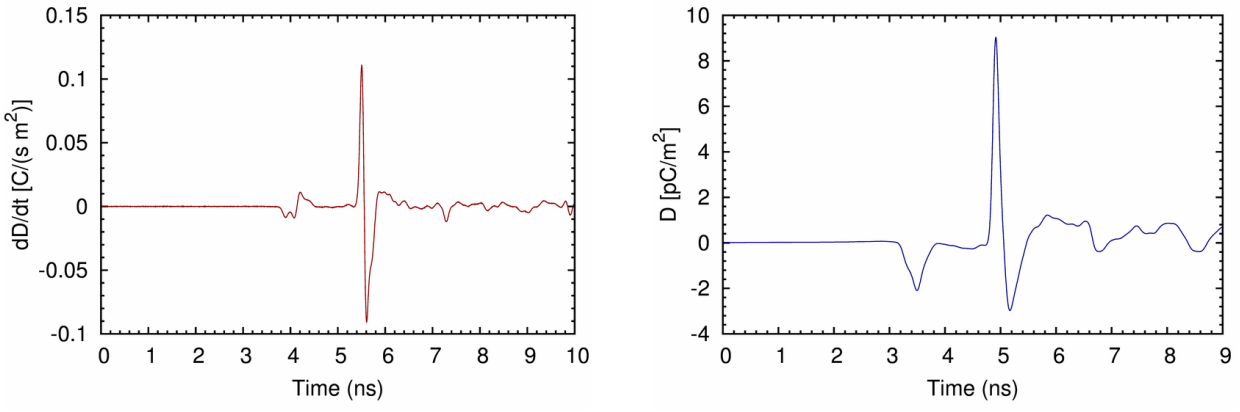

(a) Raw D-dot probe signal

(b) Intergrated D-dot probe signal

Figure 4.1: "Raw" and integrated D-dot probe signal.

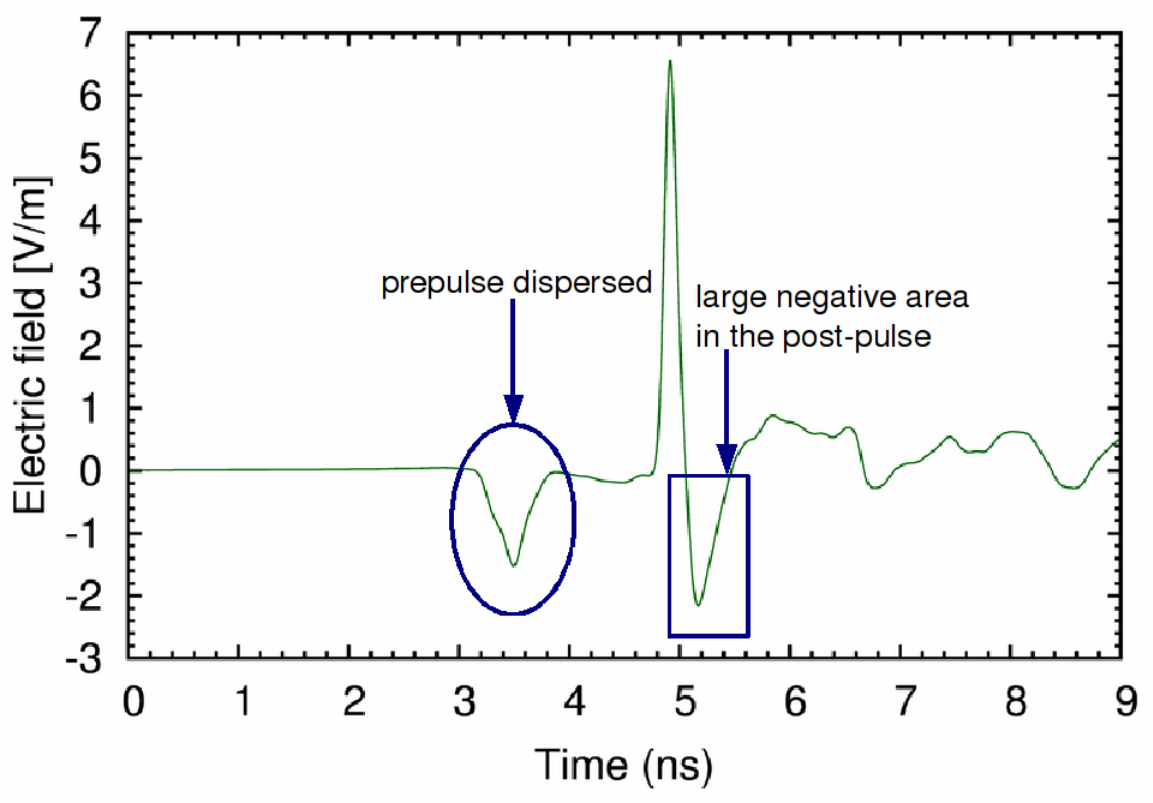

Figure 4.2: Electric field focal waveform in lens with 100 ps filter.

The "zoomed-in" view of the electric field impulse is shown in Fig. 4.3. The peak electric field amplitude is $E_{\max} = 6.557$ V/m. As in [2], the pre-pulse, impulse and post-pulse are considered as three separate events, i.e., the impulse can be considered to be super-imposed on the pre-pulse. Therefore, the amplitude of the impulse, E^{I}, is calculated with respect to the average of the start and end of the impulse event; $E_s^i = 0.0$ V/m and $E_e^i = -2.2$ V/m, as shown in Fig. 4.3, i.e.,

$$\Upsilon = \left| \frac{E_s^i + E_e^i}{2} \right| = 1.1 \text{ V/m}, \tag{4.6}$$

and

$$E^{\mathrm{I}} = E_{\max} + \Upsilon = 7.66 \text{ V/m}. \tag{4.7}$$

The FWHM, as determined numerically from the experimental data, is 127.5 ps as shown in Fig. 4.3. The large FWHM is most likely due to loss and dispersion in the lens materials (without loss and dispersion the FWHM would be 100 ps).

Figure 4.4 compares the focal impulse waveforms in air and inside the focusing lens. One observes the enhancement inside the lens. Since the half-widths of the impulse responses in air and in the lens are not identical, the electric enhancement is given by the ratio of the areas, $A =$ (half-width)(peak amplitude) $=$ FWHM $\cdot\, E_{\max}$, under the curves, i.e.,

$$\begin{aligned} A_{\text{impulse-air}} &= (85 \text{ ps})(5.44 \text{ V/m}) = 462.4 \text{ ps V/m}, \\ A_{\text{impulse-lens}} &= (127.5 \text{ ps})(7.66 \text{ V/m}) = 976.65 \text{ ps V/m}. \end{aligned}$$

The electric enhancement is $A_{\text{impulse-lens}}/A_{\text{impulse-air}} \approx 2.11$. This is much larger than the analytical estimate, $\epsilon_r^{1/4} = 8.2^{1/4} \approx 1.69$. The reason for this disagreement is due to the 85 ps FWHM of the impulse in air [2]. The analytical approximations do not consider the filtering of the lower frequencies due to the focusing of the wave, at the second focal point, in air. This results in a much higher electric enhancement as observed above. Of course, one could also simply examine the ratio of the peak electric fields inside the lens and in air, which is $7.66/5.44 = 1.408$.

The areas under the curves as obtained from numerical simulations are

$$\begin{aligned} A_{\text{impulse-air}} &= (64.569 \text{ ps})(6.2466 \text{ V/m}) = 403.337 \text{ ps V/m}, \\ A_{\text{impulse-lens}} &= (70.233 \text{ ps})(10.7248 \text{ V/m}) = 753.235 \text{ ps V/m}. \end{aligned}$$

The electric enhancement is $A_{\text{impulse-lens}}/A_{\text{impulse-air}} \approx 1.868$. This is also larger than that predicted analytically. The smaller FWHM in air and inside the lens indicates that the filtering of lower frequencies, due to the focusing of the wave at the second focal point, is taken into consideration in the numerical simulations. The enhancement obtained from the ratio of the peak focal impulse electric fields is $10.725/6.247 = 1.717$.

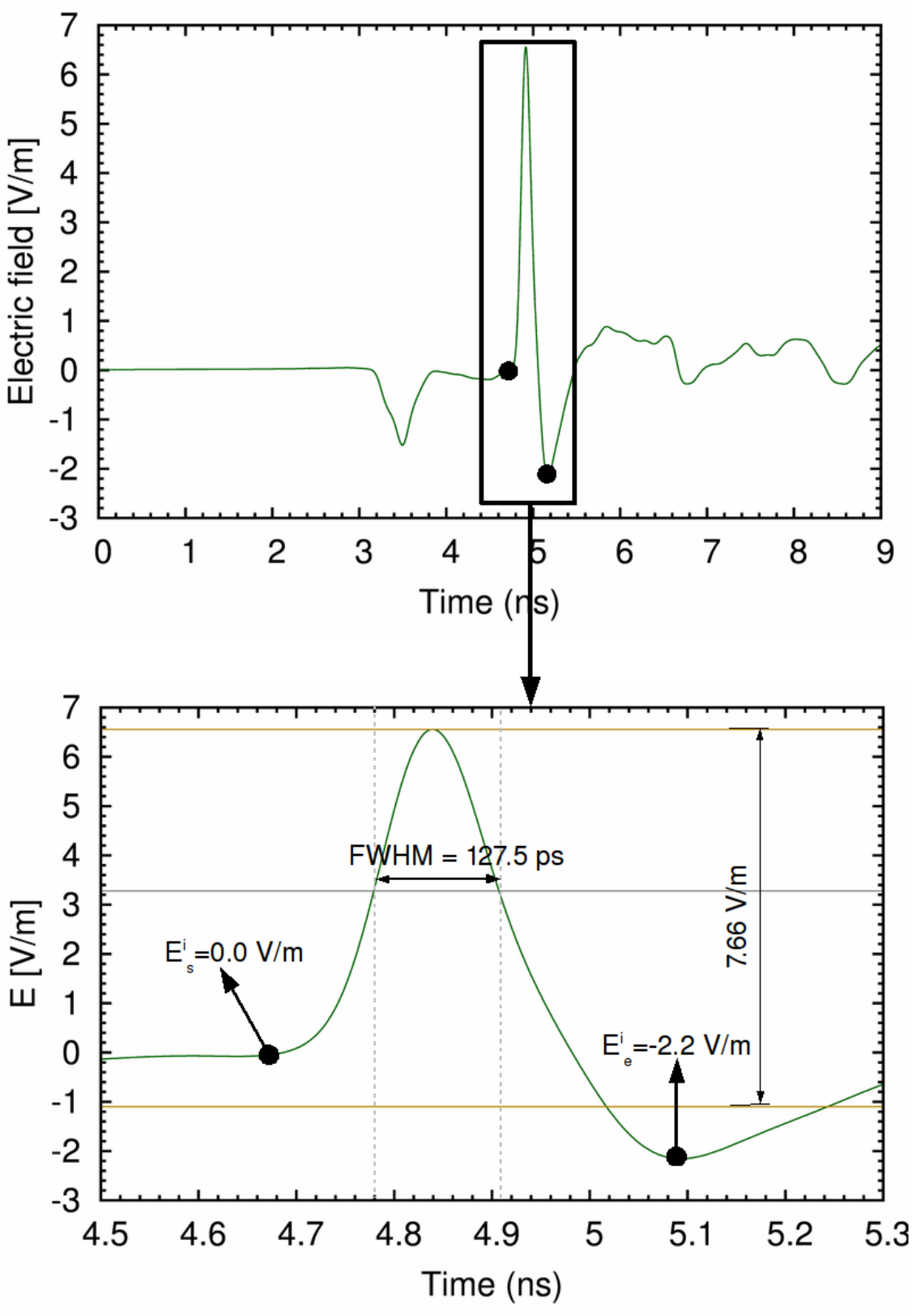

Figure 4.3: "Zoomed-in" view of electric field impulse at second focal point in lens with 100 ps filter.

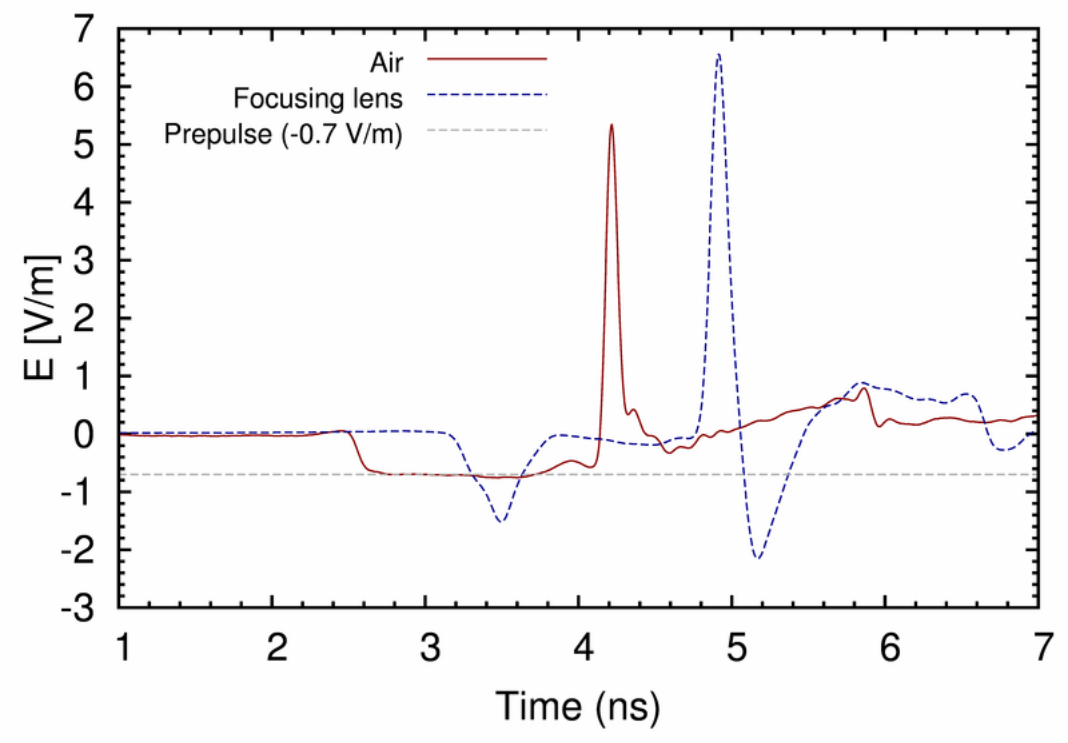

Figure 4.4: Comparison of focal impulse waveforms, at the second focal point, in air and inside the lens, with the 100 ps filter.

4.2 The focusing lens as a bandpass filter

The ratio of the magnitudes of the Fourier transform of the impulse waveforms from experiments, in the lens and in air, is shown in Fig. 4.5. The bandwidth of the lens is approximately 3 GHz, from 0.4 GHz to 3.4 GHz. Above 3.5 GHz there is almost no electric field enhancement (analytical or experimental). The focusing lens thus acts as a bandpass filter, filtering frequencies below 0.4 GHz and above 3.4 GHz. The filtering of higher frequencies is due to losses occuring in the lens materials while the filtering of lower frequencies is due to the lens geometry.

The curve in Fig. 4.5 is compared to similar results obtained from simulations in Fig. 4.6. The (average) amplification is approximately 1.7 (dotted gray line) upto a frequency of 20 GHz, as expected, since the lens materials are assumed lossless and dispersionless in the simulations. This is closer to that obtained from the ratio of the peak focal electric fields, i.e., $10.725/6.247 = 1.717$. Therefore, the analogous experimental enhancement, $7.66/5.44 = 1.408$, is considered in Fig. 4.5.

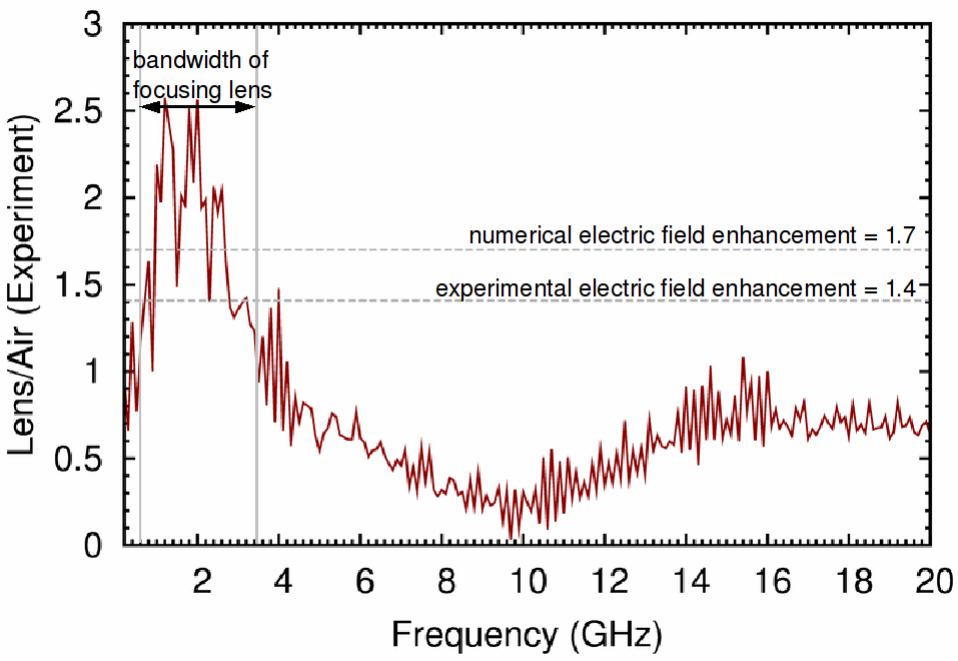

Figure 4.5: Ratio of magntitude of Fourier transform of the focal impulse waveform from experiments.

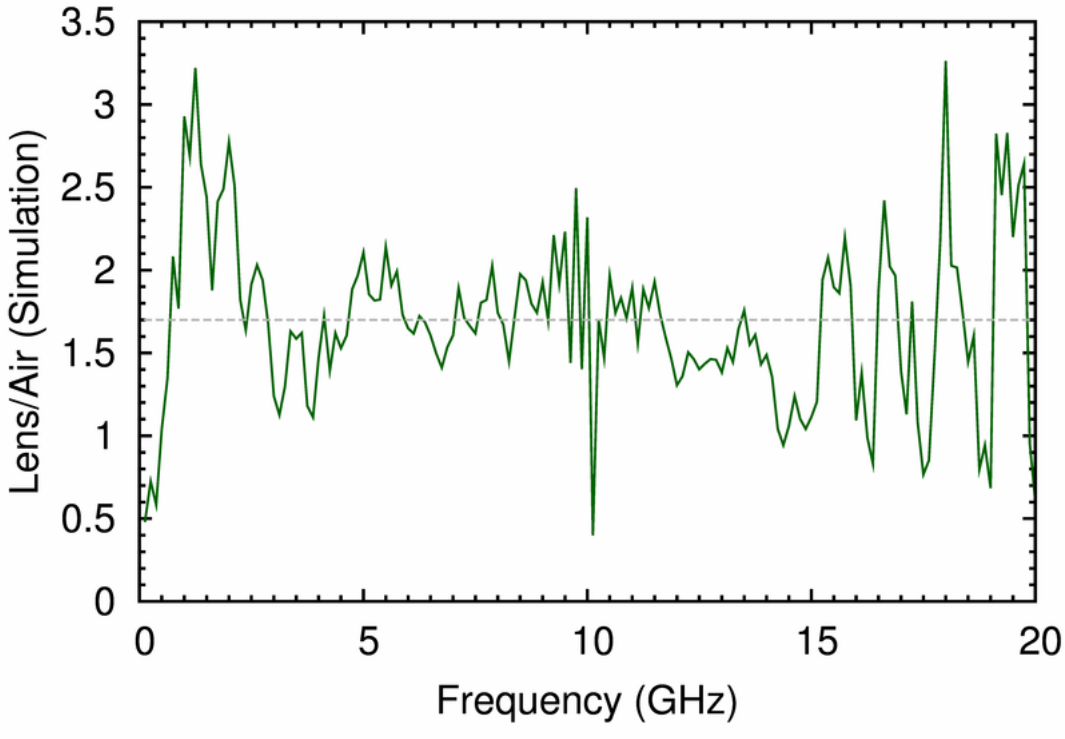

Figure 4.6: Ratio of magntitude of Fourier transform of the focal impulse waveform, from simulations, for an input pulse with 100 ps rise time. The dotted gray line is 1.66, the electric enhancement obtained with the lens.

4.3 Beam width (Spot size)

As explained in [1], the lens reduces the beam width (spot diameter) by a factor of $\epsilon_{rt}^{1/2} = 8.2^{1/2} = 2.86$ in the target medium. This is desirable in the treatment of skin cancer (melanoma). Figure 4.7 compares the experimental results of the beam width in air and in the lens. The half-power width in air is 4.397 cm and in the lens it is 1.836 cm. Therefore, the spot size in the lens is reduced by a factor of 4.397 cm/1.836 cm $\approx 2.395 \approx \epsilon_{rt}^{1/2} = 8.2^{1/2}$ as obtained from numerical simulations.

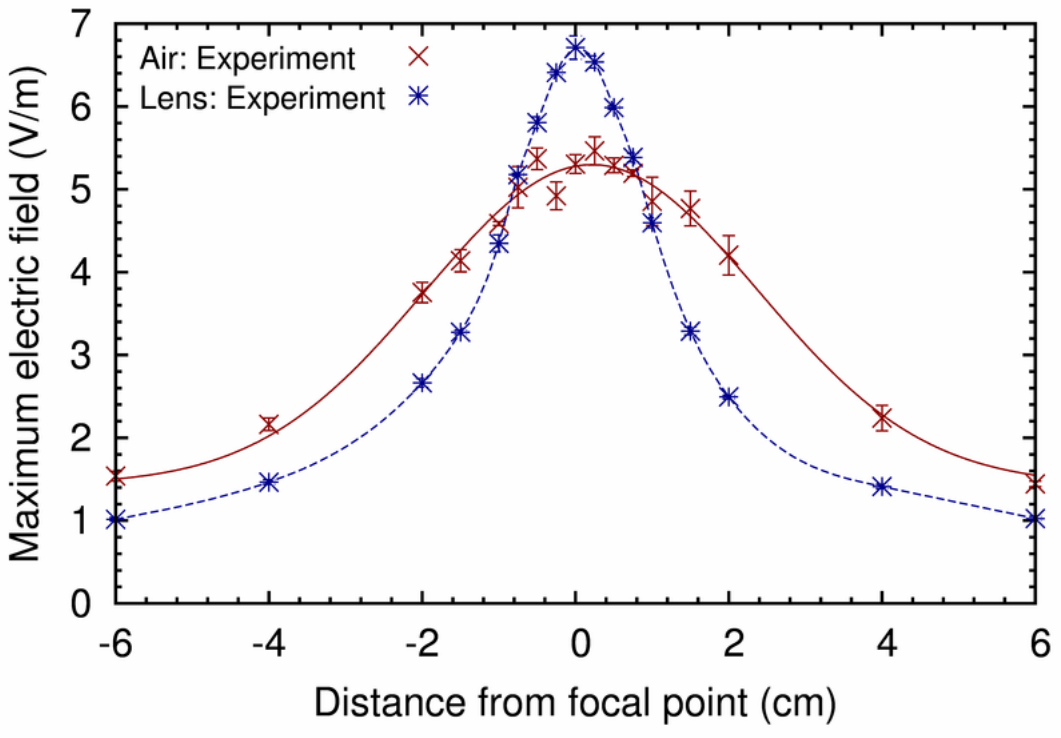

Figure 4.7: Comparison of experimental results of beam width in air and in lens.

Figure 4.8 and Fig. 4.9 compare simulation and experimental results of the beam width in air and in the lens. Errors in the experimental data are of the order of the spot size. As seen in Figure 4.8, the simulation and experiment results of the spot size in air agree very well. One observes that the geometric focal point in the lens is shifted to the right by approximately $x = +0.25$ cm. Noting that the pulse emerging from the lens is approximately 130 ps in width, mostly due to losses occuring in the lens materials, it would be appropriate to multiply the experimental peak electric fields in Fig. 4.7 and Fig. 4.9 by 1.3 (= 130 ps/100 ps).

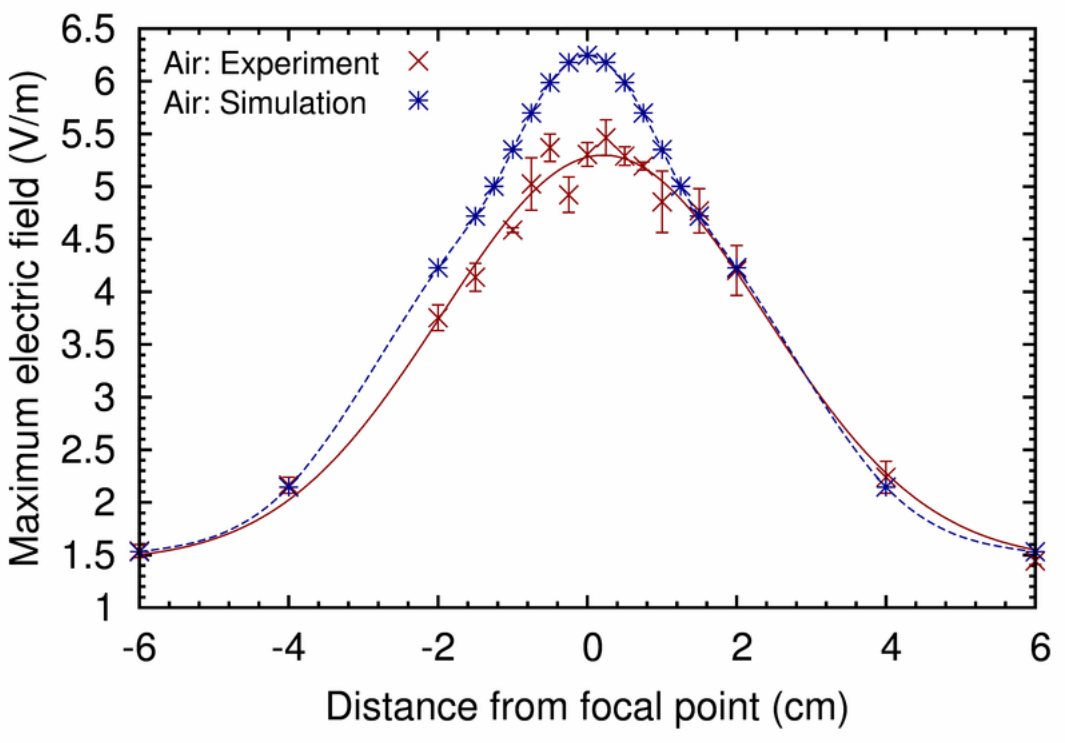

Figure 4.8: Comparison of simulation and experiment results of beam width in air.

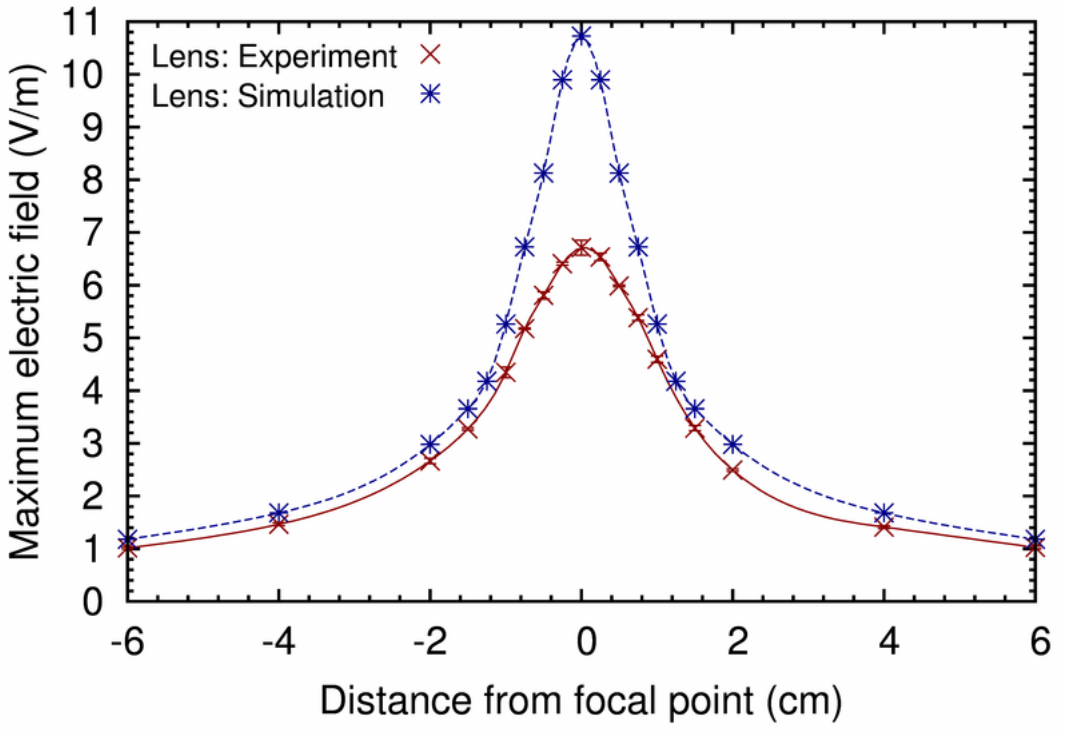

Figure 4.9: Comparison of simulation and experiment results of beam width in lens.

Table 2 summarizes and compares the spot sizes obtained from experiments and simulations.

Table 2: beam width of electric field in air and with focusing lens from Fig. 4.7 and Fig. 4.8

	Simulation	Experiment
No lens ($EFSS_{NL}$ in cm)	3.61	4.397
With Lens ($EFSS_{WL}$ in cm)	1.19	1.836
$EFSS_{WL}/EFSS_{NL}$	3.04	2.395

The spot sizes in Fig. 4.7, Fig. 4.8 and Fig. 4.9 are obtained by taking the peak electric fields, of the focal waveforms, at the respective positions. As explained in Sec. 4.1 above, a more accurate measurement is to reference the peak impulse amplitude with respect to the start and end of the impulse event. This increases the peak amplitude by

$$\Upsilon = \left| \frac{E_s^i + E_e^i}{2} \right|. \tag{4.8}$$

To accurately determine the spot size, Υ must be calculated for the impulse waveform at each position along x. However, as a first approximation, the Υ for the impulse waveforms at all x positions may be assumed to be identical to that at the focal point. In Fig. 4.10, Fig. 4.11 and Fig. 4.12 the peak electric fields are increased by $\Upsilon = 0.1$ V/m in air [2] and $\Upsilon = 1.1$ V/m inside the lens. Table 3 summarizes and compares the spot sizes obtained from experiments and simulations after the peak electric field amplitudes have been increased by E^{I}.

Table 3: Beam width of electric field in air and with focusing lens from Fig. 4.11 and Fig. 4.12

	Simulation	Experiment
No lens ($EFSS_{NL}$ in cm)	3.61	4.451
With Lens ($EFSS_{WL}$ in cm)	1.19	2.036
$EFSS_{WL}/EFSS_{NL}$	3.04	2.187

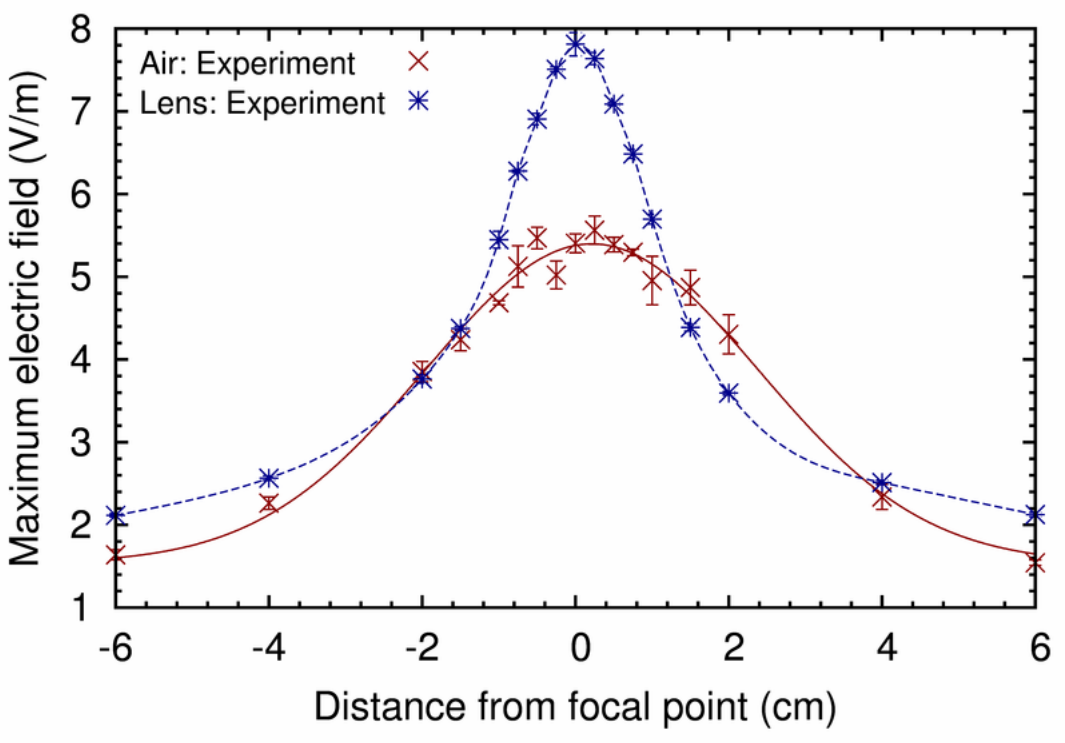

Figure 4.10: Comparison of experimental results of beam width in air and in lens.

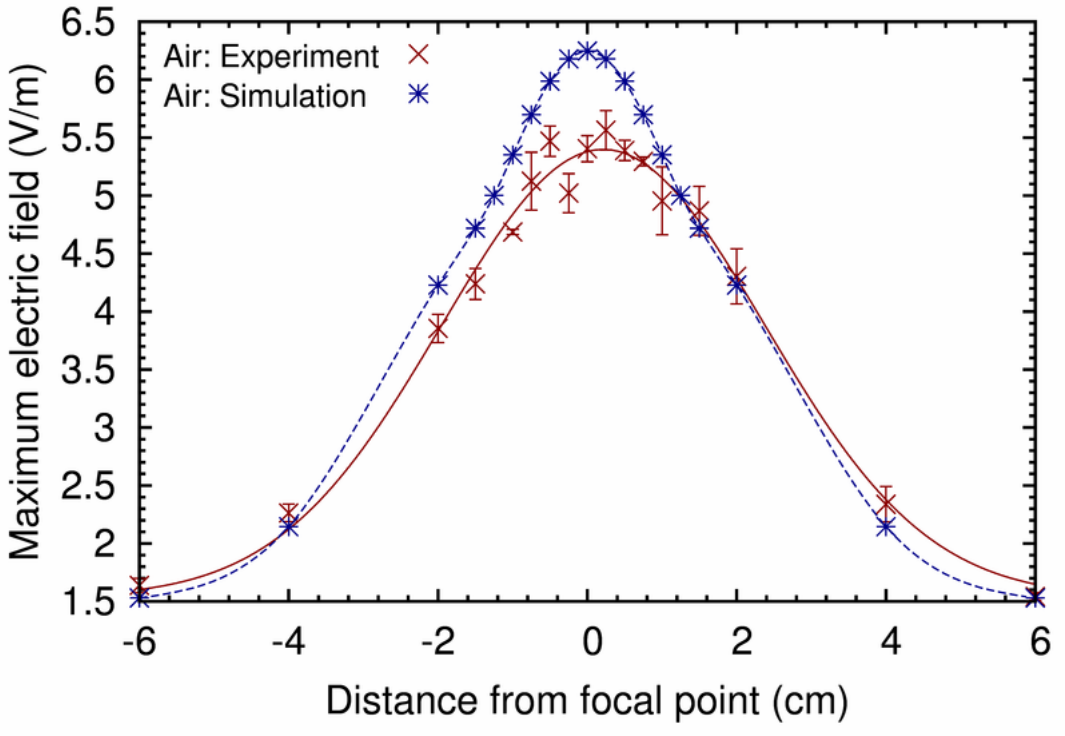

Figure 4.11: Comparison of numerical simulation and experimental results of beam width in air.

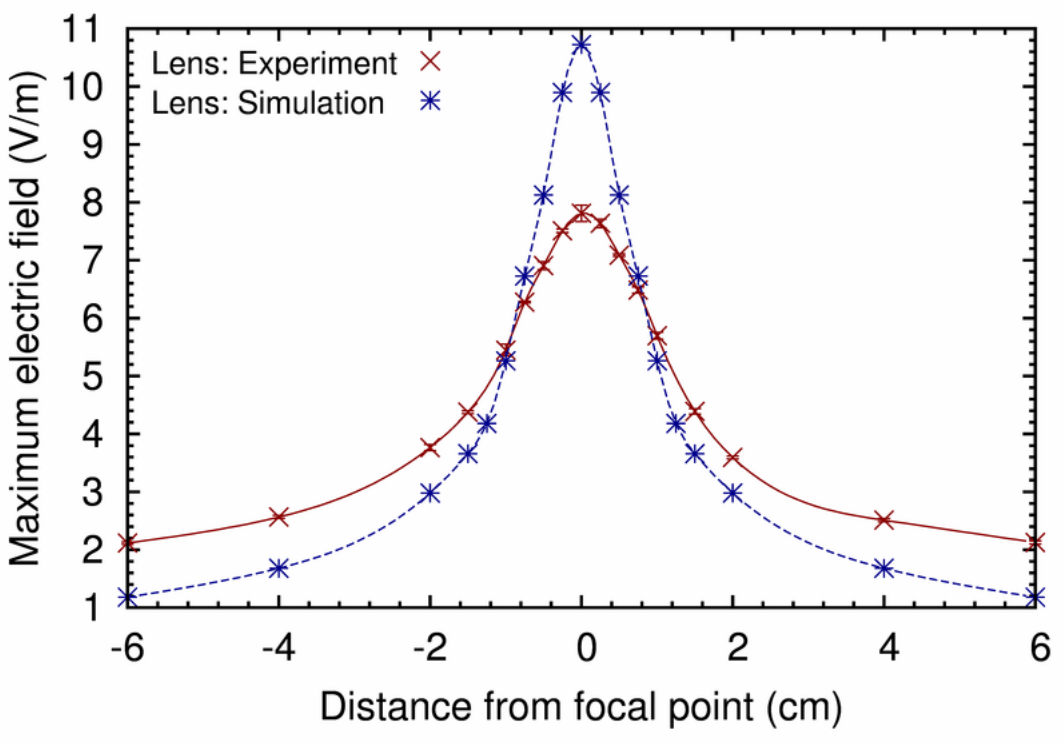

Figure 4.12: Comparison of numerical simulation and experimental results of beam width in lens.

5 Conclusions

This paper has presented the experimental results for the focal impulse waveform and beam width inside the focusing lens with a 100 ps filter. The calibration of the handmade D-dot probe [1] inside the target medium has been detailed. The electric enhancement in the focusing lens agrees well with those obtained in [1]. The focusing lens acts as a band pass filter. Loss and dispersion due to the lens materials occurs at frequencies above approximately 3.5 GHz. The beam width inside the lens is reduced by a factor of 2.2. These results agree well with those obtained from numerical simulations and analytical estimations.

References

[1] P. Kumar, S. Altunc, C. E. Baum, C. G. Christodoulou, E. Schamiloglu, and C. J. Buchenauer, "Radially Inhomogeneous Spherical Dielectric Lens for Matching 100 ps Pulses into Biological Targets," *Accepted for publication, IEEE Transactions Plasma Science, Special Issue - Nonthermal Medical/Biological Applications Using Ionized Gases and Electromagnetic Fields*, 2010.

[2] P. Kumar, S. Altunc, C. E. Baum, C. G. Christodoulou, and E. Schamiloglu, "Experimental results for the focal waveform and beam width in air with a 100 ps filter," *EM Implosion Memo 50*, July 2010.